RSC Advances

PAPER

View Article Online
View Journal | View Issue

Open Access Article. Published on 23 June 2017. Downloaded on 11/1/2025 6:44:46 AM.
This article is licensed under a Creative Commons Attribution-NonCommercial 3.0 Unported Licence.

Check for updates

Cite this: *RSC Adv.*, 2017, 7, 32275

Preparation and characterization of insensitive HMX/rGO/G composites *via in situ* reduction of graphene oxide

Chunhuan Niu, Bo Jin,* Rufang Peng,* Yu Shang and Qiangqiang Liu

Received 5th April 2017
Accepted 3rd May 2017

DOI: 10.1039/c7ra03863a

rsc.li/rsc-advances

Composites of 1,3,5,7-tetranitro-1,3,5,7-tetrazocane/reduced graphene oxide/graphite (HMX/rGO/G) were successfully prepared *via* an *in situ* chemical reduction coating method. The morphology, composition and thermal decomposition characteristic of the composites were analyzed by field-emission scanning electron microscopy (FE-SEM), X-ray photoelectron spectroscopy (XPS), X-ray diffraction (XRD), Raman spectroscopy and differential thermal analysis (DTA). rGO together with G exhibited a better desensitizing effect than fullerene and carbon nanotubes. When 1.0 wt% GO and 1.0 wt% G were added as desensitizing materials, the impact sensitivity of raw HMX decreased from 100% to 8% and the friction sensitivity decreased from 100% to 0% after *in situ* chemical reduction coating. Meanwhile, DTA results indicated that rGO and G were compatible with HMX. These combined properties suggest that rGO sheets along with graphite can be utilized as co-desensitizers in HMX explosives.

Introduction

1,3,5,7-Tetranitro-1,3,5,7-tetrazocane (HMX), a typical nitramine explosive, is extensively used as the main component of various munitions and propellants in current military applications.[1–3] Owing to the cyclic or cage structure of nitramine, HMX offers several significant advantages, such as high energy, density, burn rate, detonation velocity, and detonation pressure. The superior explosive performance of HMX, however, indicates poor sensitivity to impact, friction, shock waves, and electrical sparks *etc.* thus seriously hindering its widespread application in military and civilian fields.[4] Therefore, desensitization methods for high-energy explosives have received considerable interest. Current reports about the desensitization of high explosives have mainly focused on crystal size and shape, removal of impurities and defects *via* recrystallization, energetic cocrystals, and polymer-bonded explosives.[1,5–10] Furthermore, researches have focused on the addition of common insensitive materials, including wax, stearic acid, polymers[11–13] and carbon materials to high-energy explosives. Other studies have focused on the desensitization of high-energy explosive material *via* coating techniques, such as water slurry coating, crystallization coating, spray-drying coating, and *in situ* polymerization coating.[14–17] Nevertheless, the addition of desensitizing materials results in a poor insensitivity effect, uneven coverage, and low energy release. These problems affect the sensitivity and stored energy of the high-energy explosive material.

State Key Laboratory Cultivation Base for Nonmetal Composites and Functional Materials, Southwest University of Science and Technology, Mianyang 621010, China

Reduced graphene oxide (rGO), a new type of two-dimensional nanomaterial, occupies a unique place in nanoscience given its exceptional electrical, thermal, chemical and mechanical properties, as well as rich pore structure and large surface area.[18] These excellent properties indicate that rGO is a potential desensitizing component for high-energy explosives.[19] In recent years, extensive research has been carried out on the preparation and application of graphene nanomaterials in energetic materials.[20,21] Examples of these nanomaterials include insensitive HMX/GO composites, surface-coated insensitive HMX with Viton and GO, HMX coated with graphene oxide by electrostatic self-assembly, graphene nanoplatelet–lead styphnate composites with depressed electrostatic hazards, CL-20 hosted in graphene foam, and insensitive ε-HNIW with binders and graphite.[22–28] Some of the most important research focus is graphene nanomaterials, which can be utilized as carriers of energetic components *via* coating or encapsulation. The graphene-coated or graphene-encapsulated energetic components can form advanced nanostructures with superior performance, thus improving the safety of energetic systems.

In this study, GO together with G were selected as co-desensitizers, and through an *in situ* chemical reduction coating method, 1,3,5,7-tetranitro-1,3,5,7-tetrazocane/reduced graphene oxide/graphite (HMX/rGO/G) composites were successfully prepared. Morphological and structural characterization revealed that the surface of the HMX crystal was well coated by rGO and G, and the DTA results showed that the decomposition temperature of HMX changed little, which revealed that the added graphite and graphene oxide did not influence the energy output of HMX and were compatible with

Open Access Article. Published on 23 June 2017. Downloaded on 11/1/2025 6:44:46 AM.
This article is licensed under a Creative Commons Attribution-NonCommercial 3.0 Unported Licence.

HMX. Meanwhile, sensitivity tests also indicated that the coated energetic system expressed depressed mechanical sensitivity with a superior balance between high energetic performance and low sensitivity.

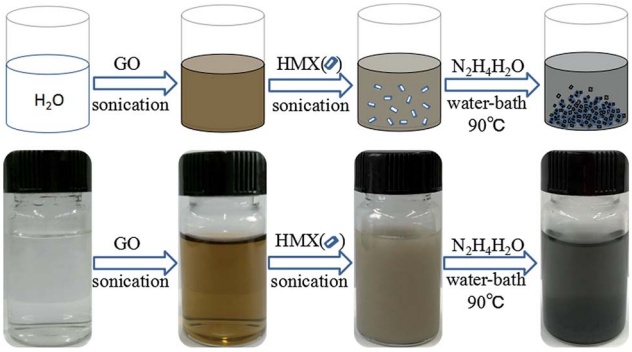

Fig. 1 Preparation procedure of HMX/rGO composite.

Results and discussion

Preparation

HMX/rGO composites were successfully prepared *via* an *in situ* chemical reduction coating method. The overall process of synthesis was simple, including three stages. The first step was the key ultrasonic stage which decided the coating effect, and the second step—the real reaction stage—was where GO was reduced by hydrazine hydrate and the *in situ* coating process occurred simultaneously. Then, the final step was the treatment of the reaction solution including centrifugation, washing, and vacuum-drying. HMX/rGO/G was also prepared *via* an *in situ* chemical reduction coating method. To highlight the desensitization effect of G, a blank experiment—the preparation of HMX/G—was executed under the same experimental conditions *via* the *in situ* chemical reduction coating method. The observable experimental phenomenon indicated the completion of sample preparation was the change in solution color and the final mixed solution contained a black precipitate after the

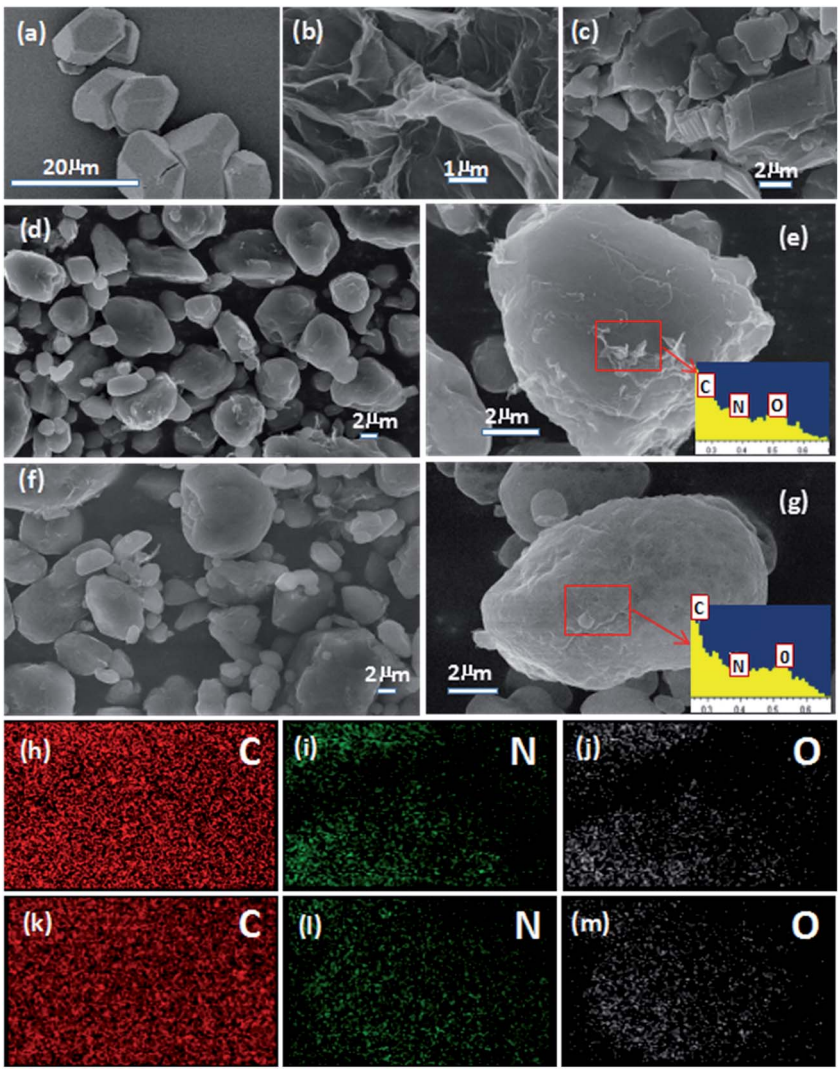

Fig. 2 SEM images of (a) HMX, (b) rGO sheets, (c) graphite, (d) HMX/rGO, (f) HMX/rGO/G EDS spectrum of HMX/rGO (e) and HMX/rGO/G (g), the corresponding elemental mapping images for C, N and O of HMX/rGO (h–j) and HMX/rGO/G (k–m).

Open Access Article. Published on 23 June 2017. Downloaded on 11/1/2025 6:44:46 AM.
This article is licensed under a Creative Commons Attribution-NonCommercial 3.0 Unported Licence.

reaction. The preparation of HMX/rGO composites and an image of the reaction solution are shown in Fig. 1. Fig. 1 also presents the preparation of HMX/rGO/G. The specific experimental details of the prepared composites are provided in the experimental section.

Morphological analysis

Field-emission scanning electron microscopy (FE-SEM) was employed to characterize the morphology and composition of the products. Fig. 2a and b show SEM images of HMX and rGO sheets. HMX was irregular and angular in shape, and the rGO sheets were flat with wrinkling and folding on the surface and edge. The SEM images of G (Fig. 2c) revealed a layered structure. The angular HMX gradually turned into the rounded HMX/rGO (2d) and spherical HMX/rGO/G (2f) *via* the *in situ* chemical reduction coating process. To further test the outcome of the coating, energy dispersive spectroscopy (EDS) was performed and elemental mapping images for C, N, and O were obtained. The EDS spectra of HMX/rGO and HMX/rGO/G are shown in Fig. 2e and g, where the ratio of C, N, and O changed because of the changing C content. The C contents of HMX/rGO (27.8%) and HMX/rGO/G (57.37%) were markedly higher than that of HMX (16.2%) because GO and G are mainly composed of carbon. The elemental mapping images of HMX/rGO and HMX/rGO/G were presented in Fig. 2(h–j) and (k–m). The C elemental mapping images of HMX/rGO and HMX/rGO/G were more uniform and compact than those of the N and O elemental mapping images. This indicated that HMX coated by rGO and G had been successfully prepared.

Structure analysis

X-ray photoelectron spectroscopy (XPS) is a well-known characterization method for the surface of microparticles. XPS efficiently detects the coating structure of numerous inorganic and organic systems.[29] To further illustrate the structure between two units, XPS was used to characterize the elemental content of the samples. The results are shown in Fig. 3. Fig. 3a and b show the XPS spectrum of HMX and HMX/rGO, in which the characteristic peaks at the binding energies of 286.9, 406.2 and 535.3 eV correspond to C 1s, N 1s, and O 1s, respectively. The peak intensities of C 1s, N 1s, and O 1s in the two spectra were different, especially the C 1s peak. This indicated that the C, N and O contents have altered. As determined *via* XPS, the actual C, N, and O contents of HMX/rGO were 46.49, 24.8 and 28.71 wt%, respectively, whereas those of HMX were 34.83, 31.46, and 33.71 wt%, respectively. These data were also consistent with the changes in peak intensity. Meanwhile, the C 1s spectra of HMX/rGO (3c) showed characteristic peaks at 284.5, 285.9, 288.1 eV which corresponded to C–C, C–OH and C=O bonds, respectively. Fig. 3d shows the C 1s spectrum of rGO that was adapted from ref. 23. Four different components at binding energies of 284.5, 285.1, 286.3, and 288.2 eV correspond to sp^2 hybridized C atoms, C–OH (alcohol/phenol), C–O–C (epoxy/ether) groups, and C=O (carbonyl/carboxyl), respectively.[30] Both HMX/rGO (3c) and rGO (3d) possessed the same peaks at 284.5 (C–C), 285.9 (C–OH) and 288.2 (C=O). Moreover, the C–C peak intensity in HMX/rGO (3c) was as strong as that in rGO (3d). These outcomes indicated that GO has been reduced to rGO and the surface of HMX crystal was also coated by rGO during the *in situ* chemical reduction coating process.

Raman spectroscopy, which is based on inelastic light scattering, is a rapid and nondestructive route for graphene characterization.[23] Carbon allotropes exhibit universal Raman shifts at around 1350 cm^{-1} and 1580 cm^{-1}, which are known as the D

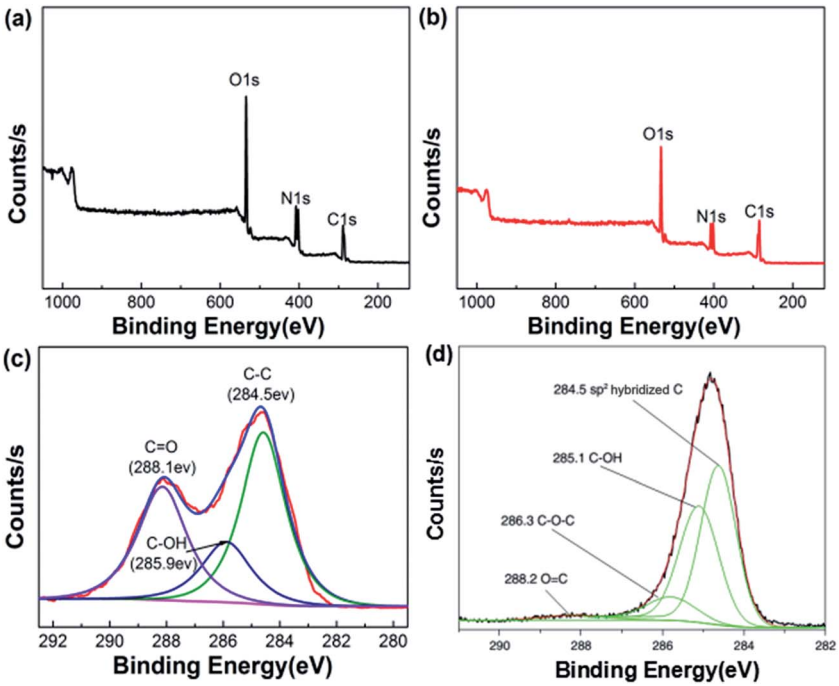

Fig. 3 XPS spectra of HMX (a) and HMX/rGO (b), the C 1s spectra of HMX/rGO (c) and reduced GO (d) adapted from ref. 23.

Open Access Article. Published on 23 June 2017. Downloaded on 11/1/2025 6:44:46 AM.
This article is licensed under a Creative Commons Attribution-NonCommercial 3.0 Unported Licence.

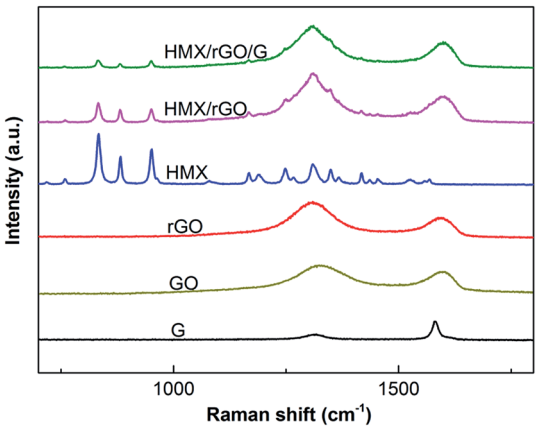

Fig. 4 Raman spectra patterns of graphite, GO, rGO, HMX, HMX/rGO and HMX/rGO/G.

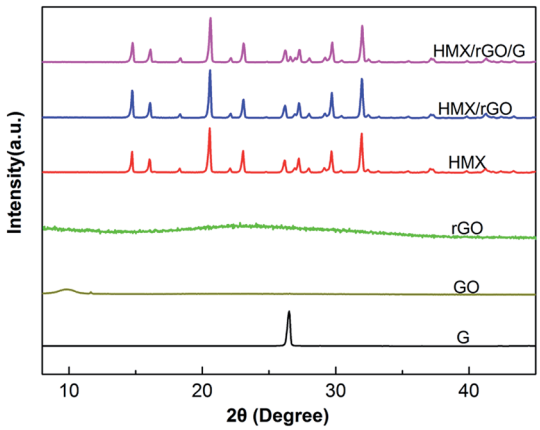

Fig. 5 XRD spectra patterns of graphite, GO, rGO, HMX, HMX/rGO and HMX/rGO/G.

and G peaks, respectively. The intensity and width of these peaks allow specific classification. The G band arises from the doubly degenerate E_g^2 phonon of sp^2 carbon atoms.[31] The D band results from disorder on the atomic level. These atomic disorders include edge effects, ripples, functional groups, and charge puddles.[31,32] In the present study, the structures of the prepared samples were investigated by Raman spectra. The outcomes of the tests are shown in Fig. 4. As shown in Fig. 4, the characteristic sharp peaks of carbon allotropes exhibit universal Raman shifts in the vicinity of the D and G peaks in the spectra of G, GO, and rGO. The change in D/G intensity ratio (I_D/I_G) between GO and rGO suggested that GO has been reduced to rGO. Both the Raman spectra of HMX/rGO and of HMX/rGO/G displayed the two stronger distinctive peaks of rGO. Meanwhile, compared with the characteristic sharp peak intensity of HMX Raman shifts at around 833 cm^{-1}, 881 cm^{-1} and 951 cm^{-1}, the characteristic sharp peak intensities of HMX/rGO Raman shifts at the three positions were distinctly reduced, and the intensities of the HMX/rGO/G Raman shifts at the same three positions were lower than those of raw HMX. These results showed that the surface of the HMX crystals may have changed and indicated that rGO along with G was coated on the surface of HMX during the *in situ* reduction coating process.

To further confirm the relationship between the two individual units and investigate the crystal structure and component state of the prepared samples, X-ray diffraction (XRD) analyses were conducted. The XRD patterns of the above samples are shown in Fig. 5. The figures show that the GO and rGO sheets possess an amorphous structure with characteristic sharp peaks at $2\theta = 10°$ and $2\theta = 22°$, whereas HMX (monoclinic, $P2_1/c$) shows a clear crystalline structure with characteristic diffraction peaks that were determined in previous work (JCPDS card no. 42-1768, respectively). After *in situ* reduction coating, the typical diffraction peaks of the explosive crystals were preserved, indicating that the coated products maintained high crystallinity. Interestingly, the diffraction intensity of several peaks changed slightly after rGO coating. Compared with that of raw HMX, the sharp peak intensity of HMX/rGO increased at $2\theta = 14.7°$ and decreased at $2\theta = 23°$. In addition, the peak intensity of HMX/rGO/G decreased at $2\theta = 23°$ and $2\theta = 27°$. Crystals in the powder samples present an original orientation distribution and this change is likely caused by rGO and graphite coating on the crystal surface. More specifically, the increased peak intensity of the composites likely resulted from the exposure and detection of crystals in their preferred orientation, leading to the variations in diffraction intensity.[16] Meanwhile, the XRD patterns of HMX/rGO and HMX/rGO/G revealed the absence of the characteristic sharp peaks of GO, rGO, and G at approximately $2\theta = 10°$, 22°, and 26°, respectively. These results confirmed that rGO with G were well composited with HMX. Similar results were also found in a previous report.[26,33]

Thermal analysis

Thermal performance is regarded as a key property for energetic materials and influences their preparation, storage, processing and application.[34,35] Therefore, the thermal stabilities of the prepared samples were investigated *via* differential thermal analysis (DTA). The DTA analyses were performed under an air flow of 50 mL min^{-1} with approximately 2 mg of sample and α-Al_2O_3 as the reference material. As shown in Fig. 6, two peaks

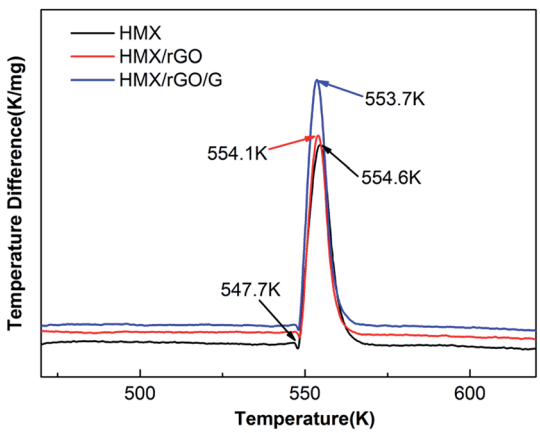

Fig. 6 DTA curves for HMX, HMX/rGO and HMX/rGO/G.

Open Access Article. Published on 23 June 2017. Downloaded on 11/1/2025 6:44:46 AM.
This article is licensed under a Creative Commons Attribution-NonCommercial 3.0 Unported Licence.

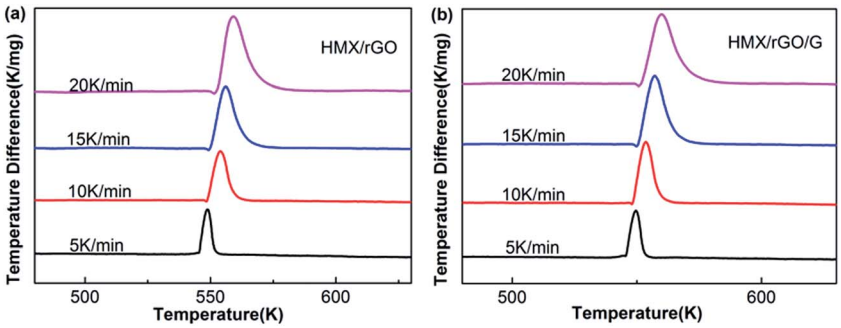

Fig. 7 DTA curves for HMX/rGO (a) and HMX/rGO/G (b) at different heating rates.

were found in the DTA curve of HMX: a sharp endothermic peak at approximately 547.7 K, which corresponds to melting; and a decomposition peak at 554.6 K. These results are consistent with the literature values.[36,37] After the addition of rGO and G, the thermal decomposition peak temperatures of HMX/rGO (554.1 K) and HMX/rGO/G (553.7 K) did not markedly change compared with the decomposition peak at HMX (554.6 K), where the change between the samples was less than 2 K, and this negligible change indicated the compatibility of rGO and G with HMX.[27,38,39]

To determine the kinetic parameters of the thermal decomposition of the samples, thermal performance was further evaluated using the Kissinger method.[40] Kissinger's equation[41,42] is presented as follows:

$$\ln\left(\frac{\beta}{T_p^2}\right) = \ln\left(\frac{AR}{E_a}\right) - \frac{E_a}{RT_p} \quad (1)$$

where β is the heating rate (K min^{-1}), T_p is the temperature of the exothermic peak (K), R is the ideal gas constant (8.314 J mol^{-1} K^{-1}), E_a is the activation energy, and A is the pre-exponential factor. The DTA analyses of prepared samples under 5, 10, 15 and 20 K min^{-1} heating rates are shown in Fig. 7. According to eqn (1), $\ln(\beta/T_p^2)$ varies linearly with $1/T_p$, yielding the kinetic parameters of the activation energy (E_a) from the slope of the straight line and pre-exponential factor from the intercept. The calculated activation energies of HMX/rGO and HMX/rGO/G were 341.2 kJ mol^{-1} (R^2 = 0.991) and 328.7 kJ mol^{-1} (R^2 = 0.992), respectively. Compared with the activation energy of HMX 350.9 kJ mol^{-1} (R^2 = 0.999),[28] the small change in activation energy of the prepared samples showed that the added rGO with G did not affect the decomposition of HMX.

Table 1 Mechanical sensitivities of HMX and prepared composites

Samples	Proportion	Impact sensitivity (%)	Friction sensitivity (%)	Reference
HMX	100	100	100	43 and 44
HMX/[60]fullerene 1	99/1	100	100	43
HMX/[60]fullerene 2	99/1	90	100	43
HMX/[60]fullerene 3	99/1	60	70	43
HMX/CNTs-1	99/1	72	76	44
HMX/CNTs-5	95/5	28	72	44
HMX/rGO	98/2	16	100	
HMX/G	98/2	40	30	
HMX/rGO/G	98/1/1	8	0	

Sensitivity analysis

Sensitivity is a key index of explosive safety and considerably influences the storage, transportation, packaging, and application of energetic materials. Therefore, an impact sensitivity test was conducted in accordance with the GJB-772A-97 standard method as follows: a 50 mg sample was placed between steel anvils and hit by a 10 kg hammer that was dropped from a height of 25 cm. Friction sensitivity was then investigated as follows: a 30 mg sample was placed between steel anvils and hit by a 1.5 kg pendulum hammer fixed on 90° tilt angle. Gauge pressure was 3.92 MPa. Twenty five samples were tested for friction sensitivity and impact sensitivity, and the explosion probability (P, %) was calculated as a sensitivity indicator. A larger P indicated higher sensitivity.[28] The sensitivity results for the samples are listed in Table 1. Furthermore, to provide a rough estimate of the desensitizing effect of rGO and G, the mechanical sensitivities of HMX/[60]fullerene and HMX/carbon nanotubes (CNTs) are summarized in Table 1. These results indicate that rGO sheets along with G present distinct advantages over [60]fullerene and CNTs as co-desensitizers in explosives.

As can be seen from Table 1, the impact sensitivities of HMX/rGO evidently decreased compared with those of raw HMX. When the added GO content was 2.0 wt%, the explosion probability of impact sensitivity decreased from 100% to 16%, but friction sensitivity did not change markedly. To decrease the friction sensitivity, we introduced G into the system. Both the impact and the friction sensitivities of HMX/G decreased, especially the friction sensitivities. With the addition of 2.0 wt% G, the explosion probability of friction sensitivity decreased from 100% to 30%. Therefore, the final formula HMX/rGO/G was synthesized. When 1.0 wt% G and 1.0 wt% GO were added, the explosion probability of HMX/rGO/G impact sensitivity decreased from 100% to 8%, and the explosion probability of HMX/rGO/G friction sensitivity decreased from 100% to 0%. This finding indicated that rGO with G as co-desensitizers

Open Access Article. Published on 23 June 2017. Downloaded on 11/1/2025 6:44:46 AM.
This article is licensed under a Creative Commons Attribution-NonCommercial 3.0 Unported Licence.

exerted an excellent desensitization effect on HMX. This desensitization effect might result from the high specific surface area of rGO, which could form a dense layer on the HMX surface and transmit heat between each HMX crystal under certain stimuli. Therefore, fewer hot spots could be generated, leading to a great reduction in the sensitivity.[45] rGO sheets can be readily extended to up to hundreds of microns in the lateral dimension.[46,47] When mechanical forces act on the explosives, larger rGO sheets are beneficial for dissipating the energy.

Conclusions

Insensitive HMX/rGO/G composites were successfully prepared *via in situ* reduction of GO. The results of SEM, XRD, and Raman spectra analysis revealed that raw HMX was evenly coated by rGO together with G. Meanwhile, the DTA results indicated that rGO and G were compatible with HMX. Compared with [60] fullerene and CNTs, rGO sheets along with G were better co-desensitizers in explosives. When 1.0 wt% GO and 1.0 wt% G were added, through *in situ* chemical reduction, the impact sensitivity of raw HMX decreased from 100% to 8% and the friction sensitivity decreased from 100% to 0%. The reasons for the insensitivity, however, are not yet fully understood. Thus, further studies should investigate desensitizing mechanisms. The results of the present study provide a route for adjusting the sensitivity of high-energy explosives.

Experiment section

General

Graphene oxide (GO, 1–2 layers) with a content of over 99%, graphite (99%) and hydrazine hydrate (85%) were purchased from the market. The raw HMX was provided by the Institute of Chemical Materials, Chinese Academy of Engineering Physics. Ultrapure water (18.25 MΩ cm) was prepared by a Millipore Milli-Q system and used throughout the experiment. Ultrasonic dispersion was conducted with an SK-250H ultrasonic bath (250 W) and centrifugation was conducted on a SF-TGL-16M high-speed refrigerated centrifuge at a rotation speed of 9000 rps for 6 minutes. Field-emission scanning electron microscopy (FE-SEM) and energy dispersive spectroscopy (EDS) images for measuring the morphology and element of the samples were made on an Ultra 55 microscope system (Zeiss, Germany). X-ray photoelectron spectroscopy (XPS) was acquired from a Thermo VG 250 (USA) instrument. X-ray diffraction (XRD) patterns were obtained by using X'Pert Pro X-ray diffractometer (PANalytical, Netherlands). Raman spectra were recorded by an Invia Raman Spectrometer (Renishaw, England) with an excitation wavelength of 785.5 nm and a wavelength range of 100 cm^{-1} to 3000 cm^{-1}. Differential thermal analysis (DTA) curves were recorded on a WCR-1B analyzer at heating rates of 5, 10, 15 and 20 K min^{-1} under an air flow 50 mL min^{-1} with the reference α-Al_2O_3. The impact sensitivity of the samples was tested with a WL-1 drop hammer impact instrument and the friction sensitivity was determined on a WM-1 pendulum friction apparatus.

Preparation of HMX/rGO

10 mg of GO (the theoretical mass fraction was 2%) was put into 50 mL of ultrapure water and ultrasonically dispersed for 1 h, until the GO was completely dispersed in water. Then, 490 mg of HMX was added into the mixed solution and uniformly ultrasonically dispersed for 1 h with the help of ultrasonic vibration. Afterwards, 200 μL of hydrazine hydrate was added into the mixed solution and the above solution was heated in a water bath at 90 °C with magnetic stirring. The reaction continued under reflux for 2 h and the reaction solution was cooled to room temperature. After centrifugation, washing, and evaporation *in vacuo* at 50 °C, 355.3 mg of HMX/rGO was obtained as a black solid with a yield of 71%.

Preparation of blank HMX/G

10 mg of graphite (G) was added into 50 mL of ultrapure water and ultrasonically dispersed for 1 h. Then, 490 mg of HMX was added into the mixed solution and uniformly ultrasonically dispersed for 1 h with the help of ultrasonic vibration. Afterwards, 200 μL of hydrazine hydrate was added into the mixed solution and the above solution was heated in a water bath at 90 °C with magnetic stirring. The reaction continued under reflux for 2 h and the reaction solution was cooled to room temperature. After centrifugation, washing, and evaporation *in vacuo* at 50 °C, 405.5 mg of HMX/G was obtained as a hoary solid with a yield of 81%.

Preparation of HMX/rGO/G

5 mg of GO and 5 mg of graphite (G) were put into 50 mL of ultrapure water and ultrasonically dispersed for 1 h, until the GO was completely dispersed in water. Then, 490 mg of HMX was added into the mixed solution and uniformly ultrasonically dispersed for 1 h with the help of ultrasonic vibration. Afterwards, 200 μL of hydrazine hydrate was added into the mixed solution and the above solution was heated in a water bath at 90 °C with magnetic stirring. The reaction continued under reflux for 2 h and the reaction solution was cooled to room temperature. After centrifugation, washing, and evaporation *in vacuo* at 50 °C, 365.6 mg of HMX/rGO was obtained as a black solid with a yield of 73%.

Acknowledgements

This work was supported by the Natural Science Foundation of China (51372211), Open Project of State Key Laboratory Cultivation Base for Nonmetal Composites and Functional (project no. 14tdfk05), Southwest University of Science and Technology Outstanding Youth Foundation (project no. 13zx9107).

References

1 A. E. D. M. van der Heijden and R. H. B. Bouma, *Cryst. Growth Des.*, 2004, **4**, 999–1007.
2 E. A. Zhurova, V. V. Zhurov and A. A. Pinkerton, *J. Am. Chem. Soc.*, 2007, **129**, 13887–13893.

Open Access Article. Published on 23 June 2017. Downloaded on 11/1/2025 6:44:46 AM.
This article is licensed under a Creative Commons Attribution-NonCommercial 3.0 Unported Licence.

3 R. L. Simpson, P. A. Urtiew, D. L. Ornellas, G. L. Moody, K. J. Scribner and D. M. Hoffman, *Propellants, Explos., Pyrotech.*, 1997, **22**, 249–255.
4 A. K. Sikder and N. Sikder, *J. Hazard. Mater.*, 2004, **112**, 1–15.
5 H. Kröber and U. Teipel, *Propellants, Explos., Pyrotech.*, 2008, **33**, 33–36.
6 R. M. Doherty and D. S. Watt, *Propellants, Explos., Pyrotech.*, 2008, **33**, 4–13.
7 X. Jiang, X. Guo, H. Ren and Q. Jiao, *Cent. Eur. J. Energ. Mater.*, 2012, **9**, 219–236.
8 O. Bolton and A. J. Matzger, *Angew. Chem., Int. Ed.*, 2011, **50**, 8960–8963.
9 Y. Bayat, S. M. Pourmortazavi, H. Ahadi and H. Iravani, *Chem. Eng. J.*, 2013, **230**, 432–438.
10 A. Elbeih, S. Zeman, M. Jungová and P. Vávra, *Propellants, Explos., Pyrotech.*, 2013, **38**, 379–385.
11 K. Cowey, S. Day and R. Fryer, *Propellants, Explos., Pyrotech.*, 1985, **10**, 61–64.
12 E. da Costa Mattos, E. D. Moreira, M. F. Diniz, R. C. L. Dutra, G. da Silva, K. Iha and U. Teipel, *Propellants, Explos., Pyrotech.*, 2008, **33**, 44–50.
13 L. Wen, S. Quancai, W. Wenbin and C. Yongke, *Propellants, Explos., Pyrotech.*, 1996, **21**, 247–250.
14 J. W. Jung and K. J. Kim, *Ind. Eng. Chem. Res.*, 2011, **50**, 3475–3482.
15 Z. Ma, B. Gao, P. Wu, J. Shi, Z. Qiao, Z. Yang, G. Yang, B. Huang and F. Nie, *RSC Adv.*, 2015, **5**, 21042–21049.
16 Z. Yang, L. Ding, P. Wu, Y. Liu, F. Nie and F. Huang, *Chem. Eng. J.*, 2015, **268**, 60–66.
17 J. Chen, J. Wang, B. Wang and H. Huang, *Chin. J. Explos. Propellants*, 2009, 28–31.
18 Y. Zhai, Z. Zhu and S. Dong, *ChemCatChem*, 2015, **7**, 2806–2815.
19 Q. L. Yan, M. Gozin, F. Q. Zhao, A. Cohen and S. P. Pang, *Nanoscale*, 2016, **8**, 4799–4851.
20 H. Wang, F. Q. Zhao and S. W. Li, *Chin. J. Explos. Propellants*, 2006, **29**, 32–35.
21 Y. L. Wang, F. Q. Zhao and J. H. Yi, *Chin. J. Explos. Propellants*, 2012, **35**, 1–8.
22 L. Yu, X. Jiang, X. Guo, H. Ren and Q. Jiao, *J. Therm. Anal. Calorim.*, 2013, **112**, 1343–1349.
23 L. Yu, H. Ren, X. Y. Guo, X. B. Jiang and Q. J. Jiao, *J. Therm. Anal. Calorim.*, 2014, **117**, 1187–1199.
24 T. Liu, C. Z. Geng, B. H. Zheng and G. Luo, CN. Pat., 106431792 A, 2017.
25 Z. Li, Y. Wang, Y. Zhang, L. Liu and S. Zhang, *RSC Adv.*, 2015, **5**, 98925–98928.
26 Z. Li, M. Zhou, T. Zhang, J. Zhang, L. Yang and Z. Zhou, *J. Mater. Chem. A*, 2013, **1**, 12710.
27 J. Wang, B. Ye, C. An, B. Wu, H. Li and Y. Wei, *J. Energ. Mater.*, 2016, **34**, 235–245.
28 R. Li, J. Wang, J. P. Shen, C. Hua and G. C. Yang, *Propellants, Explos., Pyrotech.*, 2013, **38**, 798–804.
29 K. Huang, R. Demadrille, M. G. Silly, F. Sirotti, P. Reiss and O. Renault, *ACS Nano*, 2010, **4**, 4799–4805.
30 Y. Hernandez, V. Nicolosi, M. Lotya, F. M. Blighe, Z. Sun, S. De, I. T. McGovern, B. Holland, M. Byrne, Y. K. Gun'Ko, J. J. Boland, P. Niraj, G. Duesberg, S. Krishnamurthy, R. Goodhue, J. Hutchison, V. Scardaci, A. C. Ferrari and J. N. Coleman, *Nat. Nanotechnol.*, 2008, **3**, 563–568.
31 D. Yang, A. Velamakanni, G. Bozoklu, S. Park, M. Stoller, R. D. Piner, S. Stankovich, I. Jung, D. A. Field, C. A. Ventrice and R. S. Ruoff, *Carbon*, 2009, **47**, 145–152.
32 D. Krishnan, F. Kim, J. Luo, R. Cruz-Silva, L. J. Cote, H. D. Jang and J. Huang, *Nano Today*, 2012, **7**, 137–152.
33 Z. Tang, X. Chen, H. Chen, L. Wu and X. Yu, *Angew. Chem.*, 2013, **52**, 5832–5835.
34 W. Gong, B. Jin, R. Peng, N. Deng, R. Zheng and S. Chu, *Ind. Eng. Chem. Res.*, 2015, **54**, 2613–2618.
35 Q. Yan and S. Zeman, *Int. J. Quantum Chem.*, 2013, **113**, 1049–1061.
36 C. An, J. Wang, W. Xu and F. Li, *Propellants, Explos., Pyrotech.*, 2010, **35**, 365–372.
37 M. Herrmann, W. Engel and N. Eisenreich, *Propellants, Explos., Pyrotech.*, 1992, **17**, 190–195.
38 Z. R. Liu, C. M. Yin, C. H. Y. Wu and M. N. Chang, *Propellants, Explos., Pyrotech.*, 1986, **11**, 10–15.
39 K. Luo, *Propellants, Explos., Pyrotech.*, 1996, **21**, 206–214.
40 X. Song, Y. Wang, C. An, X. Guo and F. Li, *J. Hazard. Mater.*, 2008, **159**, 222–229.
41 L. Li, X. Sun, X. Qiu, J. Xu and G. Li, *Inorg. Chem.*, 2008, **47**, 8839–8846.
42 Q. Yang, S. Chen, G. Xie and S. Gao, *J. Hazard. Mater.*, 2011, **197**, 199–203.
43 B. Jin, R. Peng, S. Chu, Y. Huang and R. Wang, *Propellants, Explos., Pyrotech.*, 2008, **33**, 454–458.
44 Y. Chi, H. Huang and J. S. Li, *International Autumn Seminar on Propellants, Explosives and Pyrotechnics*, Beijing, China, 2005, pp. 319–323.
45 Z. Yang, J. Li, B. Huang, S. Liu, Z. Huang and F. Nie, *Propellants, Explos., Pyrotech.*, 2014, **39**, 51–58.
46 C. Su, Y. Xu, W. Zhang, J. Zhao, X. Tang, C. Tsai and L. J. Li, *Chem. Mater.*, 2009, **21**, 5674–5680.
47 J. L. Sabourin, D. M. Dabbs, R. A. Yetter, F. L. Dryer and I. A. Aksay, *ACS Nano*, 2009, **3**, 3945–3954.